Title

Multimodal imaging of bacterial-host interface in mice and piglets with Staphylococcus aureus endocarditis.

Journal

Science Translational Medicine, 12(568)

Authors

Panizzi, Peter
Krohn-Grimberghe, Marvin
Keliher, Edmund
et al.

Publication Date

2020-11-04

DOI

10.1126/scitranslmed.aay2104

Peer reviewed

HHS Public Access

Author manuscript

Sci Transl Med. Author manuscript; available in PMC 2021 May 04.

Published in final edited form as:

Sci Transl Med. 2020 November 04; 12(568): . doi:10.1126/scitranslmed.aay2104.

Multimodal imaging of bacterial-host interface in mice and piglets with *Staphylococcus aureus* endocarditis

Peter Panizzi[1,†,‡], **Marvin Krohn-Grimberghe**[2,3,†], **Edmund Keliher**[2], **Yu-Xiang Ye**[2], **Jana Grune**[2], **Vanessa Frodermann**[2], **Yuan Sun**[2], **Charlotte G. Muse**[1], **Kaitlyn Bushey**[4], **Yoshiko Iwamoto**[2], **Mandy M.T. van Leent**[5], **Anu Meerwaldt**[5], **Yohana C. Toner**[5], **Jazz Munitz**[5], **Alexander Maier**[5], **Georgios Soultanidis**[5], **Claudia Calcagno**[5], **Carlos Pérez-Medina**[5,6], **Giuseppe Carlucci**[7], **Kay P. Riddell**[8], **Sharron Barney**[9], **Glenn Horne**[9], **Brian Anderson**[10], **Ashoka Maddur-Appajaiah**[11], **Ingrid M. Verhamme**[11], **Paul E. Bock**[11,$], **Gregory R. Wojtkiewicz**[2], **Gabriel Courties**[2], **Filip K. Swirski**[2], **William R. Church**[4], **Paul H. Walz**[8], **D. Michael Tillson**[9], **Willem J.M. Mulder**[5,12,13], **Matthias Nahrendorf**[2,14,15,*,‡]

[1]Department of Drug Discovery and Development, Harrison School of Pharmacy, Auburn University, Auburn, AL 36849, USA. [2]Center for Systems Biology and Department of Radiology, Massachusetts General Hospital, Harvard Medical School, Boston, MA 02114, USA. [3]University Heart Center Freiburg, 79106 Freiburg, Germany [4]Green Mountain Antibodies, Burlington, VT 05401, USA. [5]Biomedical Engineering and Imaging Institute, Department of Radiology, Icahn School of Medicine at Mount Sinai, New York, NY 10029, USA. [6]Centro Nacional de Investigaciones Cardivasculares (CNIC), 28029 Madrid, Spain. [7]Bernard and Irene Schwarz Center for Biomedical Imaging, New York University, New York, NY 10016, USA. [8]Department of Pathobiology, College of Veterinary Medicine, Auburn University, Auburn, AL, USA. [9]Department of Clinical Science, College of Veterinary Medicine, Auburn University, Auburn, AL 36849, USA. [10]Swine Research and Education Center, Department of Animal Sciences, Auburn University, Auburn, AL 36849, USA. [11]Department of Pathology, Microbiology and Immunology, Vanderbilt

[*]Corresponding author: MNahrendorf@mgh.harvard.edu.
[†]These authors contributed equally to this work.
[‡]These authors jointly supervised this work.
[$]deceased

Author contributions

P.P., M.K.-G., Y.-X.Y., J.G., V.F., Y.S. induced endocarditis in mice, imaged mice, harvested tissues, performed in vitro assays and analyzed data. P.P., E.K. and M.N. invented the imaging probes which were made and validated by E.K.. Y.I. performed mouse and pig histology. G.R.W. did optical imaging, PET/CT and MRI in mice. G.Co., M.K.-G. and Y.-X.Y. did intravital microcopy in mice. P.P., S.B., G.H., K.P.R., B.A., P.H.W., D.M.T., F.K.S. and M.N. conceived, developed and characterized the piglet endocarditis model. Pig endocarditis was induced and imaged by P.P., C.G.M., M.M.T.L., A.Me., Y.C.T., J.M., A.Ma., G.S., C.C., C.P.-M., G.Ca., K.P.R., S.B., G.H., B.A., A.M.A., I.M.V., P.E.B., P.H.W., D.M.T. and W.J.M.M.. K.B., A.M.A., I.M.V.. P.E.B., and W.R.C. developed and characterized immunotherapy. All results were analyzed and discussed by P.P., M.K.-G., F.K.S. and M.N.. P.P. and M.N. conceived, designed, and directed the study. M.N., P.P., M.K.-G., E.K., Y.-X.Y., J.G. and W.J.M.M. wrote the manuscript, which was revised and approved by all authors.

Competing interests

P.P., E.K. and M.N. are inventors on a provisional patent application (63/045,234) submitted by Massachusetts General Hospital that covers a PET and optical imaging agent for endocarditis and clotting. W.C. is an inventor on US patent (US 2018 / 0371108 A1) submitted by Green Mountain Antibodies for an antibody that detects and therapeutically blocks staphylocoagulase. K.B. is an employee of Green Mountain Antibody and W.R.C. is the owner of Green Mountain Antibody. All other authors declare no competing interests. M.N. has received consulting fees unrelated to this work from Verseau, Gimv, and IMF Therapeutics. F.K.S. has received consulting fees unrelated to this work from Verseau. P.P., E.K. and M.N. are inventors on a patent application pursued by MGH.

Data and materials availability

All data associated with this study are available in the main text or the supplementary materials.

University Medical Center, Nashville, TN 37212, USA. [12]Department of Oncological Sciences, Icahn School of Medicine at Mount Sinai, New York, NY 10029, USA. [13]Laboratory of Chemical Biology, Department of Biomedical Engineering and Institute for Complex Molecular Systems, Eindhoven University of Technology, 5612 AZ Eindhoven, The Netherlands [14]Cardiovascular Research Center, Massachusetts General Hospital, Harvard Medical School, Boston, MA 02114, USA. [15]Department of Internal Medicine I, University Hospital Würzburg, 97080 Würzburg, Germany.

Abstract

Acute bacterial endocarditis is a rapid, difficult to manage and frequently lethal disease. Potent antibiotics often cannot efficiently kill *Staphylococcus aureus (S. aureus)* that colonizes the heart's valves. *S. aureus* relies on virulence factors to evade therapeutics and the host's immune response, usurping the host's clotting system by activating circulating prothrombin with staphylocoagulase and von Willebrand factor-binding protein. An insoluble fibrin barrier then forms around the bacterial colony, shielding the pathogen from immune cell clearance. Targeting virulence factors may provide previously unidentified avenues to better diagnose and treat endocarditis. To tap into this unused therapeutic opportunity, we co-developed therapeutics and multimodal molecular imaging to probe the host-pathogen interface. We introduced and validated a family of small-molecule optical and positron emission tomography (PET) reporters targeting active thrombin in the fibrin-rich environment of bacterial colonies. The imaging agents, based on the clinical thrombin inhibitor dabigatran, bound to heart valve vegetations in mice. Using optical imaging, we monitored therapy with antibodies neutralizing staphylocoagulase and von Willebrand factor binding protein in mice with *S. aureus* endocarditis. This treatment deactivated bacterial defenses against innate immune cells, decreased in vivo imaging signal and improved survival. Aortic or tricuspid *S. aureus* endocarditis in piglets was also successfully imaged with clinical PET/magnetic resonance imaging (MRI). Our data map a route towards adjuvant immunotherapy for endocarditis and provide efficient tools to monitor this drug class for infectious diseases.

One sentence summary:

Multimodal intravital microscopy and PET imaging of *S. aureus* endocarditis can monitor adjuvant immunotherapy in mice and pigs.

Introduction

Bacterial endocarditis is an often lethal infection of the heart valves and surrounding endocardium (1). Major challenges to clinically managing endocarditis include identifying the causal pathogens, timing surgical interventions and rising bacterial resistance to antibiotics (2). To address these difficulties, we here introduce imaging tools for fundamental and translational research examining host-pathogen interactions.

Staphylococcus aureus (*S. aureus*) is the most common cause of acute endocarditis in patients (1), likely because these bacteria produce potent factors promoting bacterial virulence and survival. Historically, *S. aureus* has been differentiated from other pathogens,

such as *S. epidermidis*, through its distinct ability to clot blood (3). This directly results from *S. aureus*' production of the two redundant prothrombin activators staphylocoagulase (SC) and von Willebrand factor-binding protein (vWBp) (4, 5). SC and vWBp both bind active prothrombin through N-terminal interactions and stay locked into the vegetation through independent C-terminal binding interactions. This anchoring mechanism essentially paints vegetations with layers of thrombin-like proteolytic activity (6, 7). As a consequence, a fibrin-rich wall shields the bacterial colony against drugs and immune cells.

The coagulase-prothrombin complex binds direct thrombin inhibitors such as dabigatran (8). Here we introduce a family of dabigatran-derived small molecule imaging agents that target the SC-(pro)thrombin or vWBp-(pro)thrombin complexes residing in growing *S. aureus* vegetations. The radioisotope twin of this imaging agent family has the potential to monitor *S. aureus* endocarditis in large animals, while the fluorescent sibling enables intravital microscopy and fluorescence molecular tomography in mice. Such dabigatran analogs should be useful imaging agents given their low toxicity profile, small size, short blood half-life and high tissue permeability.

We therefore (i) synthesized and characterized dabigatran derivates labeled with either a near-infrared fluorochrome or the positron emission tomography (PET) isotope fluorine-18; (ii) used the fluorescent imaging agent in noninvasive fluorescence tomography and intravital microscopy to assess the relative distribution of thrombin activity in growing vegetations; (iii) developed a piglet model of tricuspid *S. aureus* endocarditis; (iv) demonstrated the feasibility of integrated PET/magnetic resonance (MR) imaging for detecting of *S. aureus* endocarditis using ^{18}F-dabigatran in mice and piglets; and (v) evaluated by imaging an immunotherapy that neutralizes SC and vWBp in mice with endocarditis. This therapy reduced thrombin deposition, boosted innate immune cell defense and impeded vegetation formation. Ultimately, our work furthers the development of PET imaging agents for diagnosing *S. aureus* endocarditis and provides a facile preclinical tool to accelerate the discovery of antimicrobial compounds and therapies adjunctive to antibiotics.

Results

Synthesizing imaging agents ^{18}F-DAB and DAB-VT680XL

Thrombin activation through *S. aureus* virulence factors is a key bacterial defense mechanism downstream of potential drug targets. A targeted imaging agent thus has the potential to aid first preclinical discovery and later therapeutic trials. We therefore developed an imaging agent based on the Food and Drug Administration (FDA)-approved thrombin inhibitor dabigatran (DAB), capitalizing on the high affinity and specificity of this small molecule inhibitor. We synthesized both fluorescent and radioactively labeled versions in two steps (Fig. 1A). First, we derivatized dabigatran with an amino group. The DAB-amino intermediate was then used to attach either the radioisotope 18-Fluorine (^{18}F), to yield the PET imaging agent ^{18}F-DAB, or the fluorochrome VivoTag 680XL (VT680XL), to synthesize the near infrared imaging agent DAB-VT680XL, which can be used for intravital microscopy and fluorescence molecular tomography. Mass spectrometry after liquid chromatography confirmed the identities of DAB-VT680XL (Fig. 1B) and the non-radioactive standard ^{19}F-DAB (Fig. 1C). Note that ^{18}F-DAB has a specific collection

window (Fig. 1D) to obtain the imaging agent with high radiochemical purity (Fig. 1, E and 1F).

As expected, ^{19}F-DAB's affinity for thrombin was less than the drugs argatroban and dabigatran (Fig. 1G); however, it remained sufficient for use as a sensitive imaging agent. Serial blood sampling after intravenous ^{18}F-DAB injection into mice yielded a short blood half-life of 2.0±0.6 minutes, which is typical for small molecule imaging agents that are rapidly renally eliminated (Fig. 1H). Such fast clearance is advantageous for imaging endocarditis vegetations, which are surrounded by blood. Bio-distribution studies of ^{18}F-DAB in mice documented low uptake in the normal heart and vasculature (Fig. 1I).

DAB-VT680XL binds to endocarditic vegetations

After establishing the chemical and kinetic properties of the two dabigatran-based imaging agents, we next investigated the in vivo binding of DAB-VT680XL to arterial thrombi. We induced thrombosis in the femoral artery of mice by placing a ferric chloride-soaked filter paper on the exposed artery. Using intravital microscopy and platelet visualization by injecting a fluorescently labeled antibody binding CD41, we detected DAB-VT680XL in the thrombus (Fig. 2A), whereas a control VT680XL compound (Gly-VT680XL) did not show any binding (Fig. 2B).

To test if DAB-VT680XL binds to vegetations, we induced *S. aureus* endocarditis in mice using a combination of suture insertion and intravenous injection of bacteria, as described previously (7), and injected 2 nmol of DAB-VT680XL 90 minutes prior to euthanasia. Vegetations and valve involvement were accessed by Gram staining (Fig. 3, A and B). On an adjacent tissue section, DAB-VT680XL visualized the typically fibrin-rich wall (9) that surrounds bacterial vegetation (Fig. 3, C to G). Co-staining for CD11b^{+} innate immune cells indicates that the DAB-VT680XL-positive vegetation barrier shields bacteria from the host immune response, as myeloid cells assembled in the vascular wall in front of this barrier but were unable to cross it into the bacterial colony (Fig. 3, D and G).

Noninvasively imaging *S. aureus* endocarditis in mice

Due to light waves' poor penetration depth in tissue, optical imaging is unsuitable for imaging deep tissues. We therefore developed companion fluorescent and PET imaging agents and deployed them for fluorescence molecular (DAB-VT680XL, Fig. 4, A to E) and positron emission tomography (^{18}F-DAB, Fig. 4, F to J), respectively. Fluorescence molecular tomography/ X-ray computed tomography (FMT/CT) data demonstrated high DAB-VT680XL concentration in the aortic roots of mice with endocarditis (Fig. 4, A and B), while some signal was also observed in more distal vasculature along the suture inserted to induce endocarditis, likely due to bacteria colonizing the foreign material. Ex vivo fluorescence imaging of the excised aorta co-localized DAB-VT680XL signal with bioluminescent signal from Xen29 *S. aureus* (Fig. 4C). In sham-operated control mice that were also injected with DAB-VT680XL, fluorescent background was much lower than in mice with endocarditis (Fig. 4D), while bioluminescence signal was absent (Fig. 4E). A blocking experiment with 100-fold excess intravenous injection of dabigatran preceding injection of the imaging probe DAB-VT680XL confirmed specificity of binding (fig. S1).

We observed no DAB-VT680XL enrichment in FMT/CT imaging of mice with myocardial infarction, a setting of sterile inflammation (fig. S2). If endocarditis was induced with *S. epidermidis* Xen43, the FMT/CT signal obtained from lesions was lower than with *S. aureus* Xen29 (fig. S3). PET/CT imaging after ^{18}F-DAB injection indicated binding of the PET isotope-labeled imaging agent to endocarditis vegetations (Fig. 4, F and G). Ex vivo scintillation counting of aortas confirmed high ^{18}F-DAB uptake (Fig. 4H), which co-localized on autoradiography with bacteria-derived bioluminescent signal (Fig. 4, I and J). To explore the utility of this imaging approach in other sites of infection, we imaged mice that developed renal *S. aureus* lesions. Twenty-four hours after injection, we observed DAB-VT680XL accumulated in infected kidneys (fig. S4).

S. aureus endocarditis in piglets

Ideally, molecular imaging probes that show satisfactory performance in mice are next tested in a large animal model. This step enables testing the approach using clinical imaging equipment. Perhaps even more importantly, host defense processes differ considerably between mice and large animals or humans. We employed two piglet models of acute *S. aureus* endocarditis: one affecting the tricuspid and the other the aortic valve. To mimic the typical pathogenesis of right heart endocarditis in patients, we subcutaneously implanted a vascular port into newly weaned piglets, inserting the central line into the right external jugular vein. The central line was then advanced via the superior vena cava into the right ventricle under fluoroscopy guidance. Six hours after implantation, we injected 4-8x10^8 colony forming units (CFU) bioluminescent *S. aureus* into the port. Over the course of 10 days, piglets developed typical clinical signs of endocarditis, including fever (103.5-106.5 °F) and heart murmurs. Bacteria presence on the porcine tricuspid valve was verified by hematoxylin and eosin staining (Fig. 5A) and staphylococcal cells were identified by Gram staining (Fig. 5B).

We subsequently characterized this *S. aureus* endocarditis piglet model by clinical cardiac MRI on a 3 Tesla human scanner. We observed the development of two to four differently sized tricuspid endocarditis lesions in the right ventricles of piglets on days 10-11 after bacterial injection (Fig. 5C, Movies S1 and S2). Autopsy confirmed endocarditis vegetations, the morphology of which were reminiscent of those typically found in patients (Fig. 5D). Further, administering fluorescent DAB-VT680XL into the piglets' ear veins allowed visualization of endocarditis vegetations, as the probe's fluorescent signal co-localized with bacterial bioluminescence (Fig. 5, E to H).

For induction of left-sided endocarditis, the aortic valve was damaged with a cytology brush after gaining vascular access via the carotid artery, followed by intravenous injection of 5-8x10^8 CFU bioluminescent *S. aureus*. Piglets with left-sided endocarditis deteriorated clinically faster than piglets with right-sided endocarditis. We therefore imaged them on day 7 after disease induction. Cardiac MRI revealed development of aortic valve lesions (Fig. 5, I and J). Volumetric assessment of piglet hearts with right- and left-sided endocarditis indicated that the right ventricular ejection fraction was lower in piglets with tricuspid disease (Fig. 5K). Ex vivo bioluminescence signal co-localized with lesions on autopsy, which enriched DAB-VT680XL after intravenous injection (Fig. 5, L to P).

Encouraged by the PET data obtained in mice and optical DAB-VT680XL signal in piglets with endocarditis, we initiated a proof-of-concept PET/MR imaging study, a step typically taken if a molecular imaging probe performs as desired in small animals. To that aim, we developed an integrated PET/MR cardiac imaging protocol on a clinical scanner to simultaneously acquire high-resolution morphological information and radiotracer distribution in piglet hearts. We injected the PET imaging probe ^{18}F-DAB into three piglets with left- or right-sided endocarditis, respectively. PET/MRI revealed focal enrichment of the PET imaging agent in the aortic (Fig. 6, A and B) and tricuspid valves (Fig. 6, C and D). Autoradiographic ^{18}F-DAB signal co-localized with bacterial bioluminescence arising from vegetations (Fig. 6, E to G). Taken together, these data indicate that combining molecular PET imaging with cardiac MRI's soft tissue contrast, anatomic detail and functional capabilities may provide complementary diagnostic information to monitor and manage endocarditis.

We proceeded to compare the fluorescence in aortic versus tricuspid vegetations of piglets injected with DAB-VT680XL. We found that the target-to-background ratio was higher in aortic valve vegetations when compared to tricuspid disease (fig. S5A), which was matched by the higher bioluminescence signal in aortic lesions (fig. S5B). This difference in imaging signal may relate to bacterial load, supported by a positive correlation between bacterial bioluminescence signal and DAB-VT680XL binding across vegetations examined in both valves (fig. S5C). We speculate that these differences may have been caused by the faster clinical disease progression and the earlier imaging time point in piglets with left-sided endocarditis.

Antibody immunotherapy disrupts vegetation anatomy and improves mouse survival

Staphylocoagulase (SC) and von Willebrand factor-binding protein (vWBp) are virulence factors that *S. aureus* employs to activate the clotting cascade. The resulting fibrin wall protects bacterial colonies from the host's immune system (7). We thus hypothesized that combined antibody-mediated inhibition of these two factors would disrupt *S. aureus'* ability to form fortified vegetations. Monoclonal antibodies raised against NH_2-terminal peptides of SC (GMA-2105) and vWBp (GMA-2150), which we engineered in mice, were tested for specificity by immunoblotting. The western blot data indicate excellent specificity and no cross-reactivity of the GMA-2105 antibody with vWBp or cross-reactivity of GMA-2510 with SC (Fig. 7, A to C). Clotting assays demonstrated that targeted antibodies reduce fibrinogen conversion to fibrin in a concentration-dependent manner for both anti-SC and anti-vWBp therapies (Fig. 7, D and E). Treating mice with these monoclonal antibodies led to reduced DAB-VT680XL signal in FMT/CT imaging (Fig. 7, F and G), thereby indicating that therapeutically inhibiting SC and vWBp reduces active thrombin in bacterial colonies. Injecting neutralizing antibodies improved the survival of mice with endocarditis (Fig. 7H).

To explore how this treatment acts mechanistically, we imaged vegetations using DAB-VT680XL and intravital microscopy. The heart valves in living mice are difficult to approach with a microscope objective. We therefore established *S. aureus* vegetations in the femoral artery by inserting a suture and then intravenously injecting *S. aureus* expressing red fluorescent protein (RFP). This formed femoral artery vegetations that were comparable to

the anatomy observed in the aortic valves of mice (Fig. 7, I and J). Specifically, we observed a central RFP^+ bacterial colony surrounded by DAB-VT680XL signal highlighting a thrombin-rich layer (Fig. 7J). Staining neutrophils with intravenously injected fluorescent antibody targeting Ly6g indicated that neutrophils were unable to penetrate the capsule around RFP^+ bacteria (movie S3). Treatment with antibodies neutralizing SC and vWBp disrupted the DAB-VT680XL-stained capsule around RFP^+ bacteria, thereby granting neutrophils access to invade the *S. aureus* colony (Fig. 7I, movie S4).

Discussion

Acute endocarditis, including heart valve infection caused by *S. aureus*, is difficult to manage, potentially deadly and on the rise (1, 2, 10). Here we introduce imaging tools to monitor host-*S. aureus* interactions and a strategy for adjuvant immunotherapy that neutralizes virulence factors and improves survival in mice.

Imaging agent co-development enables multimodal sensing of optical and radioisotope probes. We developed the PET agent ^{18}F-DAB because PET is the most sensitive and translatable molecular imaging modality, as demonstrated by its clinical track record (11-13). The limitations of PET imaging include relatively low spatial resolution and high costs. Co-developing the fluorescent agent DAB-VT680XL with the same affinity ligand provides cellular resolution data for molecular targets imaged by PET. In conjunction with fluorescence molecular tomography, a quantitative imaging method available for non-invasive mouse studies, DAB-VT680XL proved useful in a preclinical neutralizing antibody trial in mice. A lower imaging signal in endocarditis vegetations echoed therapy-induced survival benefits, suggesting this imaging biomarker may predict survival. We speculate that in a clinical scenario, PET imaging with ^{18}F-DAB could track therapeutic efficiency in a trial of candidate drugs similar to the SC- and vWBp-neutralizing antibodies that we tested here in mice. If further development of this therapeutic strategy leads to a human trial and clinical use, PET imaging with ^{18}F-DAB could identify patients in need of therapy or monitor therapeutic effects. The PET/MRI data in piglets with endocarditis indicate that combining molecular PET with MRI is particularly informative, as MRI provides outstanding soft tissue contrast and sufficient temporal and spatial information to visualize *S. aureus* vegetations. Given its capacity for bedside use, facile Doppler assessment of valve function and lower cost, echocardiography will remain a mainstay for serially monitoring acute endocarditis. However, molecular PET/MRI, using either ^{18}F-DAB or other radioactive probes previously reported by others (14-17), has the potential to improve antibiotic selection and guide timing and extent of surgical interventions during key disease stages.

In contrast to other endocarditis imaging agents, ^{18}F-DAB and DAB-VT680XL do not directly bind bacteria but rather report on *S. aureus*' interaction with the host's clotting system, which contributes to biofilm formation (9). This fibrin-rich wall protects the bacterial colony against host immunity and — in combination with exopolysaccharides, extracellular DNA and other factors — hinders penetration of antibiotics (18). Our data indicate that ^{18}F-DAB and DAB-VT680XL avidly bind to this critical vegetation component. Using DAB-VT680XL in intravital microscopy visualized innate immune cells'

inability to penetrate the wall, swarm into the vegetation and kill *S. aureus*. Treatment with antibodies against SC and vWBp decreased DAB-VT680XL uptake, and myeloid cells were able to enter the vegetations. Prior work has demonstrated a similar trend for dabigatran therapy *in vitro* (19, 20); however, our microscopy data provide in vivo evidence of such host-pathogen interactions.

Noteworthy limitations related to the introduced PET/MR imaging approach include that the probe not only binds to vegetations but also to sterile thrombi. Clinically, differentiating between thrombus and vegetation can be difficult. Given this limitation, the presence of typical vegetation anatomy on MRI or clinical signs, as per the modified Duke criteria (21), may remain vital for interpreting PET signal. Another clinically relevant point that remains to be explored is prosthetic valve endocarditis, especially since metallic implants may cause MRI artifacts. Further, the imaging probe developed here targets specific host-pathogen interactions. Bacterial strains that do not enter those are outside the imaging probe's target range. Finally, the imaging target is specific to well-controlled, rare processes that occur in acutely forming clots and in the vegetation-host interface. The target abundance, and the resulting target-specific PET isotope concentration is therefore lower than what is commonly obtained with imaging agents of broader specificity such as ^{18}F-FDG, warranting further optimization in large animals prior to first-in-human studies.

We chose to work with 3-week-old piglets because these smaller animals are easier to handle and less costly than adults. In general, swine disease models are considered similar to human pathologies and thus an attractive intermediate step for drug discovery and imaging agent development. Because it relies on two archetypical endocarditis triggers in humans, namely a combination of an indwelling intravenous catheter or aortic valve damage with bacteremia, this animal model is particularly relevant to human disease. In addition to helping test therapeutics and imaging approaches in a human-like setting, the piglet model could be useful for research on surgical management, a potentially life-saving treatment still in need of optimization and standardization (1). As pig hearts are similar to humans' in size and anatomy, experiments in pigs with endocarditis could address questions such as when and how to best replace an infected valve or remove a vegetation and explore minimally invasive, catheter-based strategies.

S. aureus's co-evolution with the human immune system endowed the bacteria with several efficient countermeasures against host defenses. These include bacterial factors that kill cells, inhibit the complement system, impede neutrophil and macrophage migration, evade phagocytosis and facilitate bacterial survival after phagocytosis (9). Some virulence factors promote colonization of indwelling catheters by generating a biofilm. Typically, *S. aureus* endocarditis vegetations activate the host's clotting system to anchor the colony and surround it with a protective fibrin mesh. Upstream interventions that curtail bacterial virulence rather than host clotting factors could ultimately be a safer alternative. Indeed, we detected decreased thrombin in mouse endocarditis vegetations after treatment with antibodies that neutralize SC and vWBp. In line with studies using knock-out bacteria (22), we observed that vegetations still evolved and mice succumbed eventually; nevertheless, antibody treatment prolonged survival while DAB-VT680XL signal decreased in the lesions and innate immune cells invaded bacterial colonies. Due to the differences between the

mouse and human immune systems and prior failures to translate antibody therapeutics for *S. aureus* infections from mouse to man (23), it is unclear if the introduced antibody neutralization of staphylocoagulase and von Willebrand factor-binding protein will work in patients until this has been tested, and if such therapy is efficient if initiated during later disease stages. Thus, our data indicate that future work should investigate combining immunotherapy with antibiotics, a dual strategy that aims to augment the host's innate immunity and kill bacteria.

Materials and Methods

Study design

The studies were designed to develop PET/MRI imaging probes for bacterial endocarditis. Initial optical and nuclear imaging in mice was followed by validation in a cohort of piglets subjected to either right- or left-sided endocarditis. The rationale was to improve imaging tools for monitoring host-pathogen interactions. Formal power estimations were not performed, however the number of mice included per study (n=6) was based on prior endocarditis imaging in mice (7). Mice were randomly assigned to disease and treatment groups. Investigators were not blinded to group allocation. Wherever possible, studies were repeated at least once. The number of animals used and experimental replicates performed are stated for each experiment in the figure legends.

Bacteria

Xen29 and Xen36 are both bioluminescent strains of coagulase-positive methicillin-susceptible *Staphylococcus aureus* (MSSA). Xen 43 is *S. epidermidis* strain. All Xen strains were purchased from PerkinElmer Inc.. *S. aureus*$^{RFP+}$ is a fluorescence version of methicillin-resistant *S. aureus* USA 300, NE1260R JE2 pckA::rfp that was obtained from Dr. J. Bose of the University of Kansas Medical Center (24). Briefly, strains were cultured in liquid brain heart infusion broth under constant shaking at 150-200 rpm at 37 °C. For injecting the animals, overnight cultures were diluted 20-fold in sterile Dulbecco's phosphate buffer saline without calcium or magnesium (PBS, Lonza). The injections' approximate CFU counts were assessed by light scattering at 600 nm using a Shimadzu UV-2101PC spectrophotometer according to the manufacturer's guidelines. Prior to injection, bioluminescence production was confirmed using a bioluminescence imager (FujiFilm LAS-1000) set to 10 min integration time. Post injection, true CFU numbers were verified by serial plating on 5% sheep blood agar (Hardy Diagnostics) and expression of either the bioluminescent or fluorescent reporter gene was confirmed by imaging the agar plates. To maximize microbe pathogenicity for the porcine models, the Xen strain with strongest bioluminescence in the piglets was selected after a limited screen, and the porcine-passaged strain was cultured from a port abscess. All piglet experiments use this porcine-primed Xen36 strain.

Mouse endocarditis

To induce mouse endocarditis, we followed protocols for artery isolation surgery, 4.0 suture material insertion and *S. aureus* infection as previously reported (7). A 4-0 suture was advanced through the surgically exposed right carotid artery into the left ventricular outflow

tract and fixed in place. After a 24 hour recovery period, $1x10^6$ CFU *S. aureus* in 100 μL PBS were injected through the tail vein. Continual endothelial damage to the aortic valve caused by the indwelling suture allowed the bacteria to attach and form vegetations. All animal experimentation and cohort size determination were approved in advance by the Massachusetts General Hospital's Subcommittee on Research Animal Care.

Mouse renal infection

Mice (n=14 mice) were anesthetized with isoflurane (1-3% / 2 L O_2) and received $6x10^7$ CFU of *S. aureus* Xen 36 in *5*0 μl sterile phosphate buffered saline by intravenous injection. Mice were imaged for bioluminescence signal in the region of the kidneys starting at 48 hrs post infection. Mice (n=8) showing apparent kidney infection were separated and half of those animals received the DAB-VT680XL (10 nmol) by intravenous injection. All mice were imaged at 24 hrs after probe injection, when unbound DAB-VT680XL was excreted, and compared to non-infected control animals that only received the DAB-VT680XL injection (n=3). Imaging entailed collection of both bioluminescence (300 s exposure time) and fluorescence (675 nm excitation and 720 nm emission filters) using an IVIS Lumina XRMS system (PerkinElmer Inc.). Mice were euthanized and confirmatory in situ and ex vivo images were also collected. All experimentation was approved by the Institutional Animal Care and Use Committee for Auburn University.

Piglet endocarditis

A total of 36 newly weaned piglets (16-20 days old, weighing 10-15 Ib) were purchased from the Swine Research and Education Center at Auburn University for use in model development (bioluminescence imaging (BLI) only), fluorescence probe co-localization, and clinical PET/MRI studies. The animals were acclimated for 5-7 days prior to central-line implantation surgery. Piglets were sedated with dexmedetomidine (Dexdomitor; Zoetis) and butorphanol. An intravenous catheter was placed and anesthesia was induced using a combination of ketamine (10 mg/kg; Ketaset; Zoetis), dexmedetomidine (20 mcg/kg) and butorphanol (0.4 mg/kg). A line block of 0.5 % lidocaine (Xylocaine-MPF; Fresenius Kabi USA) was placed prior to making a 3-4 cm incision just lateral to the midline. A combination of sharp and blunt dissection was used to identify and isolate the left jugular vein and then to create a subcutaneous pocket for the vascular access port (VAP; 5Fr ClearPort; Access Technologies). The vascular port consisted of a titanium outlet with a silicone septum and catheter. A small jugular venotomy was made and a 0.025 guide-wire was introduced into the vascular lumen. The polyurethane VAP catheter was placed over the guide wire and advanced into the right ventricle under fluoroscopic guidance. Correct positioning of the catheter was confirmed using multiple injections of radiopaque contrast under fluoroscopic observation. Ports were implanted in the front right region of the neck. Once the desired catheter positioning was confirmed, the VAP catheter was secured within the jugular vein with several circumferential sutures of 3-0 polypropylene (Prolene; Ethicon). The catheter tubing was cut to an appropriate length and connected to the VAP that was then secured within the subcutaneous pocket with multiple polypropylene sutures. The surgical site was lavaged with saline and closed with 3-0 poliglecaprone 25 (Monocryl; Ethicon) in the subcutaneous and intra-dermal layers. A 22-gauge Posi-grip Huber point needle was placed into the VAP, continued patency was confirmed and the VAP was heparin-

locked. The VAP site was marked with a permanent skin marker for ease of injection. The piglets then recovered from anesthesia. Analgesia was provided with carprofen (2.2 mg/kg per os every 12 hrs; Rimadyl; Zoetis) and butorphanol (0.2-0.4 mg/kg, intramuscularly every 4-6 hrs). At 6-8 hours following surgery, piglets were injected with 4-8x10^8 CFU of *S. aureus* Xen 36 (PerkinElmer Inc.) through the VAP using a Huber needle. Thereafter the port was flushed with 5 mL sterile PBS.

For aortic valve endocarditis, piglets were similarly prepared but the aorta was accessed via the left carotid artery. Aortic valve damage was induced by repeated passing of a 2.5 mm diameter cytology brush (Endoscopy Support Services) through the valve. The brush was positioned under fluoroscopy guidance aided by repeated contrast injection. A venous leg catheter was used to administer anesthesia and the *S. aureus* Xen 36 inoculum (5-8 x 10^8 CFU) followed by a bolus 60 mL sterile saline flush.

For optical studies, piglets were injected with 0.4 μmol DAB-VT680XL in 2 mL sterile PBS via the ear vein using a 25-gauge butterfly. Animals were euthanized 10-12 hours later and BLI and fluorescence reflectance imaging (FRI) performed immediately following necropsy using an IVIS Lumina XRMS imaging system (PerkinElmer). For PET/MRI, piglets were transferred to Mt. Sinai Hospital. All experimentation and the transport were approved by the Institutional Animal Care and Use Committee for Auburn University under protocol AU# 2016-2860.

Synthesizing fluorescent and fluorine-18 labeled dabigatran

The fluorescent and nuclear thrombin-specific imaging agents are derived from the FDA-approved thrombin inhibitor dabigatran. Synthesizing both agents requires converting the parent compound's carboxylic acid functionality to an amine, which can be further modified with either a fluorochrome or ^{18}F-prosthetic group.

Synthesizing Dabigatran-NH_2

Dabigatran (50 mg, 106 μmol) was suspended in dimethylformamide (DMF, 4.0 mL) in a 20-mL vial with a magnetic stir-bar, to which *N*-Boc- 2,2′-(ethylenedioxy)diethylamine (105 mg, 424 μmol) and EDC (265 mg, 1.38 mmol) were then added. After stirring for 3 h, the reaction mixture was concentrated to dryness, re-dissolved in DMSO:H_2O (2.0:0.1 mL) and subjected to reverse phase chromatography, resulting in 50 mg for a 67.2 % isolated yield of Dabigatran-NH-Boc. LC-ESI-MS(+) m/z = 702.5 [M+H+]+. Dabigatran-NH-Boc was dissolved in H_2O:MeCN (1:1, 400 μL), and then HCl (4 M) in dioxane (1 mL) was added. The homogeneous solution was stirred at room temperature for 30 min and the reaction was concentrated by rotovap to give 41 mg, a 95.6 % yield, of Dabigatran-NH_2 as a colorless solid. LC-ESI-MS(+) m/z = 602.4 [M+H+]+; LC-ESI-MS(−) m/z = 600.4 [M−H+]−.

Synthesizing DAB-VT680XL

Dabigatran-NH_2 (0.5 mg, 0.7 μmol) was dissolved in DMF (12 μL) in a 1.5-mL centrifuge tube and added to VivoTag680 XL-NHS ester (1.0 mg, 0.7 μmol) in DMF (100 μL). After 3 h, this mixture was concentrated to dryness then redissolved in H_2O/MeCN (10:1, 110 uL)

and subjected to C18 reverse-phase HPLC purification. The combined HPLC collections were concentrated to give 1.1 mg of product, a 75.6 % yield. LC-ESI-MS(−) m/z = 917.4 ([M-2H+]/2)−, m/z = 611.2 ([M-3H+]/3)−.

Synthesizing ^{19}F-DAB

Dabigatran-NH_2 (4 mg, 6.7 μmol) was dissolved in DMF (100 μL) and triethylamine (3 μL) in a 1.5-mL centrifuge tube and treated with *N*-succinimidyl-4-fluorobenoate (3 mg, 12.5 μmol) in DMF (50 μL). After 4 h the mixture was concentrated by rotary evaporation and subjected to HPLC purification resulting in 4.1 mg of ^{19}F-Dabigatran, a 68% yield. LC-ESI-MS(+) m/z = 724.6 [M+H+]+, 746.6 [M+Na+]+.

Synthesizing ^{18}F-DAB

The prosthetic group *N*-succinimidyl-4-[^{18}F]-fluorobenzoate (^{18}F-FSB) was synthesized following the automated procedure of Scott and Shao (25), adapted for a Synthra RN Plus automated synthesizer (Synthra GmbH) operated by SynthraView software. Starting with [^{18}F]-F-, n.c.a., (~1772 MBq, 50 ± 4 mCi), ^{18}F-SFB was prepared in 25.0 % isolated yield in 100 min. Dabigatran-NH_2 (4 mg, 6.7 μmol) dissolved in acetonitrile (500 μL) and triethylamine (4 μL) was reacted with ^{18}F-SFB (447 MBq, 12 ± 3 mCi) at 65°C for 5 min, cooled and subjected to C18 reverse-phase HPLC using a Machery-Nagel Nucleodur C18 Pyramid 250x10 mm Vario-Prep column eluted with 75:25 water-acetonitrile (100 mM ammonium formate) at 5.5 mL/min and a 254 nm UV detector and radiodetector connected in series. ^{18}F-Dabigatran was synthesized in 10.7 % isolated yield (189 MBq, 5.1 ± 0.2 mCi) and at 99 ± 0.9 % radiochemical purity.

^{18}F-Dabigatran for piglet imaging was produced using a GE FX2N automated synthesizer (GE Healthcare). A QMA cartridge containing cyclotron-produced [^{18}F]fluoride (~30 GBq, 0.81 ± 0.05 Ci) was eluted with a solution containing 9 mg 4,7,13,16,21,24-hexaoxa-1,10 diazabicyclo[8.8.8]hexacosane (Kryptofix [2.2.2]); 0.08 mL 0.15 M K_2CO_3 and 1.92 mL acetonitrile into a 5 mL reaction vial. Solvents were removed azeotropically at 110 °C under a slight flow of helium. Then, *N*-succinimidyl-4-[^{18}F]-fluorobenzoate (^{18}F-SFB) was synthesized in 30 % isolated yield (as described in previous section) and reacted with Dabigatran-NH_2 (4 mg, 6.7 μmol) dissolved in acetonitrile (500 μL) and triethylamine (4 μL) at 65°C for 5 min. The reaction mixture was purified by HPLC using a C-18 semi-preparative column (Luna C-18, 250 x 10 mm, 5 μm - Phenomenex) and isocratic elution with 90:10 water (75 mM ammonium formate)/ethanol at 5 mL*min^{-1} and a 254 nm UV detector. ^{18}F-Dabigatran was synthesized in 8 ± 1.2% decay corrected radiochemical yield (2.3 ± 1.1 GBq, 0.06 ± 0.03 Ci, at room temperature (RT) for 32 min) and at > 98 % radiochemical purity. Purity was assessed via Radio-HPLC using a C-18 analytical column (Atlantis T3, 100Å, 250 x 4.6 mm, 5 μm - Waters, Milford, MA, USA, RT = 9.8 min).

Thrombin activity assay

To confirm that modification did not inhibit binding activity, VT680XL and ^{19}F-labeled dabigatran were examined with the SensoLyte AFC Thrombin Assay Kit (AnaSpec). Thrombin cleaves the substrate, releasing 7-amido-4-trifluoromethylcoumarin, which was monitored at excitation/emission = 380/500 nm.

^{18}F-DAB blood half-life

To determine the blood half-life of the fluorine-18 (^{18}F)-labeled imaging agent derived from the thrombin inhibitor dabigatran (^{18}F-DAB), blood from ^{18}F-DAB-injected mice was collected by retro-orbital bleeding and sampled with gamma-counting. Under isoflurane (1.5-3 %) anesthesia, ^{18}F-DAB was injected via tail vein (approximately 250 μCi in 100 μl PBS) in 12-week-old 6 C57BL/6 mice. Mice were kept on a heated stage (37 °C) under isoflurane anesthesia and bled 20 μl 1-2, 5, 10, 15, 30, 60 and 120 minutes after probe injection. Blood samples were weighed and residual radioactivity in the samples was measured using a gamma-counter and the percent injected dose per gram blood (%IDGB) was computed. Blood half-life was derived from fitting %IDGB to the one compartment pharmacokinetic equation $C(t) = C(o)e^{-kt}$ whereas C(t) is %IDGB at time t and k is the rate constant. Half-life is denoted as $t_{1/2} = \frac{ln(2)}{k}$.

Intravital microscopy of thrombi in the femoral artery

We used intravital microscopy to visualize DAB-VT680XL binding to freshly formed thrombi. Arterial thrombosis was induced by applying ferric chloride solution (500 mM concentration; Sigma) on the exposed femoral artery of mice. Fluorescently conjugated anti-CD41 mAb (Biolegend) was injected via tail vein to label platelets in vivo before thrombosis induction. DAB-VT680XL and control fluorochrome VT680XL were injected intravenously 5 min after thrombosis induction. Images were acquired with IVM (Olympus) in vivo.

Intravital microscopy of vegetation in the femoral artery

A 12-0 Ethicon suture material was inserted into the saphenous artery, advanced into the femoral artery and fixed in position while maintaining sufficient blood flow. Mice were allowed to recover for 6 hours before injection of 10^6 CFU *S. aureus*$^{RFP+}$ bacteria in 100 μl PBS. 6 hours after bacteria administration, SC- and vWBp-neutralizing mAb (GMA-2105 and GMA-2510, Green Mountain Antibodies) or isotype IgG-control antibodies were injected. 90 minutes before imaging, neutrophils were labeled by injecting 15 μg fluorescein isothiocyanate (FITC) anti-mouse Ly-6G antibody (Clone 1A8, BioLegend) and the vegetation was stained by injecting 2 nmol DAB-VT680XL. All injections were done via tail vein. Intravital microscopy was performed 24 hours after bacteria injection. Mice were anesthetized using 1-2 % isoflurane, then placed on a heated (37 °C) stage for imaging, and the wound was reopened. Imaging was done using an Olympus (IV100) microscope with a water-immersion objective (UMPlanFL N 20x NA 0.50, Olympus). Three channels were recorded (Ly-6G FITC, 488 nm excitation; RFP, 561 nm excitation; DAB-VT680XL, 647nm excitation) to generate z-stacks at 2 μm steps. Image post-processing was performed using ImageJ software.

FMT/CT

On day 3 after suture insertion and 48 hours after injection of either 1x10^6 CFU *S. aureus* Xen29 in 100 μl PBS or PBS only for the sham group, FMT/CT imaging was performed. To this end, mice were injected with 2 nmol of the fluorescent imaging probe and imaged 2 hours later using an FMT-2500 LX Quantitative Tomography Imaging System (PerkinElmer). After excitation at 680 nm and emission collection at 700 nm, a three-

dimensional dataset containing fluorescence concentration per voxel was reconstructed. FMT imaging was accompanied by hybrid X-ray CT angiography (Inveon PET-CT, Siemens). Image fusion was achieved using Osirix software and fiducial markers on a dedicated multimodal imaging cassette frame, as described previously (26). During CT acquisition, IsoVue 370 was infused at 50 μl/min through a tail vein catheter. The CT was reconstructed using a modified Feldkamp cone beam reconstruction algorithm (COBRA, Exxim Inc.), bilinear interpolation and a Shepp-Logan reconstruction filter. Voxels were scaled to Hounsfield units. The isotropic spatial resolution was 110 μm for CT and 1 mm for FMT. Fused data sets were used to place regions of interest in the left ventricular outflow tract and the aortic valve region. After FMT/CT, underwent ex vivo fluorescence imaging of excised aortas on an OV-110 epifluorescence microscope (Olympus). The same setup was used to evaluate the effects of SC und vWBp-neutralizing mAb treatment. Six hours after bacteria injection, either SC und vWBp-neutralizing mAb or unspecific IgG-control antibodies were injected.

Fluorescence reflectance imaging and histology

Excised aortas were imaged side-by-side with controls using epifluorescence microscope (OV-110, Olympus). The tissue was then fixed in 4 % paraformaldehyde (PFA) for at least 12 hours, embedded in optimal-cutting-temperature compound and flash-frozen in an isopentane / dry ice bath. Hematoxylin and eosin (H&E), Gram staining (Sigma-Aldrich) and immmunofluorescence staining for CD11b were performed to verify the presence of *S. aureus* bacteria and myeloid cells on the aortic valve. Fluorescence microscopy (Eclipse 80i, Nikon) was performed to investigate microscopic DAB-VT680XL localization in the vegetation, and bright field images were scanned and analyzed using a Nanozoomer 2.0RS (Hamamatsu).

PET/CT imaging in mice

On day 3 post surgery, animals were injected with 250 μCi of ^{18}F-DAB and imaged by PET-CT 1.5 hours later. We used an Inveon small animal PET-CT scanner (Siemens), a threedimensional ordered subsets maximum likelihood with maximum a posteriori (OSEM3D/MAP) algorithm with 2 OSEM and 18 MAP iterations to reconstruct into three-dimensional images. The CT was performed prior to the PET scan. The PET voxel size was 0.796 × 0.861 × 0.861 mm, for a total of 128 × 128 × 159 voxels. Standard uptake values (SUV) were obtained from manually drawn regions of interest in the invent research workplace software environment. Following PET/CT imaging, the aortic root was excised, counted on a Wallac wizard 3 gamma counter to obtain percent injected dose per gram tissue (%IDGT) and imaged for bioluminescent signal. This was followed by overnight exposure on an autoradiography cassette. Plates were read on a Typhoon 9400 Variable Mode Imager (GE Healthcare). Target to background of both the bioluminescent signal and autoradiography were quantified using manual ROI's of the aorta and background in Amira software (ThermoFisher Scientific).

Generating monoclonal antibodies that neutralize SC and vWBp

The murine monoclonal antibodies against synthetic peptides corresponded to the N-terminal residues 1 through 10 of either SC or vWBp from *S. aureus* Newman D2 Tager 104

strain (27). Corresponding peptides were synthesized with an additional C-terminal cysteine that conjugated to keyhole limpet hemocyanin (KLH) and ovalbumin (OA) using *m*-maleimidobenzoyl-*N*-hydroxysuccinimide ester (28). To generate these monoclonal antibodies, mice were injected on day 1 with KLH-peptide conjugate (100 μg) in complete Freund's adjuvant. On days 17, 27 and 42, mice were injected with KLH-peptide conjugate (50 μg) in incomplete Freund's adjuvant. Serum titers from each mouse were determined by solid-phase ELISA, and spleen cells from the mouse with the highest serum titer were fused to NS1 myeloma cells on day 162, as described using polyethylene glycol (29, 30). Hybridoma were selected using hypoxanthine, azaserine and thymidine. Fusion clones were screened by solid-phase ELISA with peptide-OA coated microtiter plates. Selected clones showing signal above ~2x-background were expanded, re-screened, sub-cloned three times by limiting dilution and stored in liquid nitrogen. SC-specific antibodies were designated GMA-2105 and others specific for vWBp were designated GMA-2510. Hybridoma cells were grown in Hybridoma-SFM media (Gibco) and antibodies purified by protein G affinity chromatography. Purified antibody was sterile-filtered and stored at 4 °C. Antibody aggregation was ruled out by size exclusion chromatography on an S-300 column and dynamic light scattering with a Zetasizer Nano-S instrument (Malvern Panalytical). The isotype of each respective antibody was independently verified using/via goat anti-mouse isotype-specific antibody (Bethyl Laboratories) using a MagPix (Luminex).

Antibody specificity for SC and vWBp

Western blot confirmed specificity of prothrombin activation-specific monoclonal antibodies. Previously characterized recombinant proteins (5, 31) were subjected to SDS gel electrophoresis with lanes corresponding to (1) vWBp-(1-263), (2) vWBp-(1-474), (3) SC-(1-325),(4) SC-(1-660) and (5) protein standards with indicated molecular weights. The elaborated proteins were transferred to PVDF membrane for western blot analysis to probe the specificity and cross-reactivity of the monoclonal antibodies targeting the critical N-termini of either SC or vWBp. The same blot was probed with either the anti-vWBp monoclonal antibody (GMA-2510) (5 μg/mL) or the anti-SC (GMA-2105) (10 μg/mL) for 1 hour at 4 °C. Following primary antibody treatment, blots were washed and probed with horseradish peroxidase-labeled rabbit anti-mouse IgG that lacked the constant region and then imaged for chemiluminescence substrate oxidation using a Fuji-Films LAS1000. The blot was stripped between primary antibody challenges. Finally, since the antibodies were intended to be used together, we verified that GMA-2510 and GMA-2105 would have additive functions in recognizing these *S. aureus* virulence factors. To accomplish this, the blot was probed with the both the SC and vWBp neutralizing antibodies and then stained for total mouse IgG content using an anti-mouse IgG (H+L)-FITC polyclonal antibody. The blot was imaged for fluorescence using a Fuji-films FLA5100 with the 473 laser and LBP channel.

Fibrinogen turbidity assays

Cleavage of fibrinogen by either prothrombin●vWBp-(1-263) or prothrombin●SC-(1-325) complexes was monitored from the increase in turbidity at 450 nm at 25 °C in 50 mM Hepes, 110 mM NaCl, 5 mM $CaCl_2$, 1 mg/mL polyethylene glycol (PEG) 8000 (pH 7.4) buffer by using a SpectraMax 340 PC 384 plate reader (Molecular Devices Inc.). Individual

reaction conditions were tested to determine the effect of the respective antibodies on the ability of either vWBp or SC to activate prothrombin and subsequently cleave of fibrinogen. GMA-2510 (anti-vWBp Ab) was incubated with vWBp-(1-263) and GMA-2105 (anti-SC Ab) was incubated with SC-(1-325) for 25 minutes at 25 °C prior to addition of prothrombin. The 3 components were then incubated together for an additional 25 minutes at 25 °C prior sub-sampling into the turbidity assay. The vWBp assays had final concentrations of 75 nM prothrombin●vWBp(1-263) complex with either 0 nM, 300 nM or 1.5 μM anti-vWBp ab. The SC assays had 15 nM prothrombin●SC(1-325) complex with either 0 nM, 50 nM, or 300 nM anti-SC ab. Fibrinogen (1.5 mg/mL) was added simultaneously to initiate all reactions. Progress curves were collected over time ranges necessary to observe total substrate depletion under the positive control conditions.

Survival study

To determine the potentially beneficial impact of eliminating prothrombin activation by bacteria, we simultaneously administered either both GMA-2105 and 2510 mAbs or an isotype control mAb (Green Mountain Antibodies, Burlington, VT). Endocarditis was induced in 30 mice, which were randomized to treatment groups. Six hours post surgery, the mice received GMA-2105, GMA-2510 or isotype-labeled mAbs by intraperitoneal injection. Mice were kept under normal husbandry without further treatment except for pain management with buprenorphine as needed until death occurred, humane endpoints were reached or up to day 7 after injection of the $1x10^6$ CFU *S. aureus*.

MRI of piglets

Left ventricular ejection fraction was quantified from retrospectively gated short-axis cardiac cine MR images (Siemens 3T Biograph mMR). Acquisition parameters for cine short axis stacks were as follows: repetition time (TR) 56.24 ms, echo time (TE) 3.32 ms, number of averages 2, 24 or 30 slices, 25 cardiac frames, 3 mm slice thickness, no interslice gap, flip angle 12, spatial resolution 0.94x0.94 mm^2. Retrospective electrocardiogram (ECG) gating was used to acquire the images. Regions of interest (ROIs) were manually segmented with Osirix MD v 9.5.1 and exported using the ‘Export ROIs’ Osirix plugin. The cine acquisition contains a total of 600 or 750 images from 24 slices with 25 cardiac frames per slice. Right ventricle vegetations were quantified from an ECG triggered axial T2 weighted turbo spin echo (TSE) stack using the following acquisition parameters: TR 1125-1485 ms, TE 76 ms, number of averages 4, 11-24 slices, 3 mm slice thickness, no interslice gap, spatial resolution 0.94x0.94 mm^2. ROIs were manually segmented with Osirix MD v 9.5.1. ROIs were exported using the ‘Export ROIs’ Osirix plugin. Vegetations were segmented as high intensity areas within the right ventricle while excluding the catheter whenever possible.

PET/MRI of piglets

Eight piglets underwent imaging with a clinical PET/MR system (Siemens 3T Biograph mMR). The piglets received an intravenous injection of ^{18}F-DAB (51.8 and 25 MBq, respectively) 90 minutes before PET acquisition. Piglets were intubated and placed on the scanner bed under isoflurane anesthesia at 1.5-2 % by inhalation, and were oxygenated throughout the PET/MR imaging experiment. Vital parameters were monitored. A 6-channel body matrix product coil was used for signal reception. Following scout scans, a static

thoracic PET was performed for 60 minutes while simultaneously acquiring cardiac and T2 weighted TSE anatomical MR images as detailed above. Attenuation correction of PET images was performed by using a vendor-built-in Dixon MR-based attenuation map (MR-AC) with 4 tissue compartments (soft tissue, fat, lung and air). Images were reconstructed using a three dimensional ordinary Poisson ordered subsets expectation maximization (OP-OSEM) algorithm with point-spread-function (PSF) resolution modeling, using 3 iterations and 21 subsets and filtered with a 4 mm Gaussian filter.

Autoradiography of piglet samples

After euthanasia, animals were perfused and heart samples were excised. To determine radiotracer distribution, digital autoradiography was performed by placing tissue samples in a film cassette against a phosphorimaging plate (BASMS-2325, Fujifilm) for 12.5 hours at −20 °C. Phosphorimaging plates were read at a pixel resolution of 25 μm with a Typhoon 7000IP plate reader (GE Healthcare). Quantification was carried out using ImageJ software.

Statistical analysis

Results are reported as mean ± standard error of mean (SEM). Statistical analysis was performed using GraphPad Prism 7 software (GraphPad Software, Inc.). Normal distribution of variables was tested using the Kolmogorov-Smirnov-test or the D'Agostino-Pearson omnibus normality test. Data were analyzed by parametric tests if normal distribution was detected. An unpaired student t-test was applied for two-group comparisons and data presented as mean ± s.e.m. with significance indicated by $*P < 0.05$, $**P < 0.01$, $***P < 0.001$ and $****P < 0.001$. If more than two groups were compared, one-way analysis of variance (ANOVA) analysis and Bartlett's test for equal variances was used. If data were non-normally distributed, differences were evaluated using an unpaired, nonparametric Mann-Whitney test. A log-rank test was applied in the survival study. Significance level in all tests was 0.05. Raw data are provided in data file S1.

Supplementary Material

Refer to Web version on PubMed Central for supplementary material.

Acknowledgements

For help with radiochemistry, we acknowledge H.-Y. Kim at Massachusetts General Hospital and R. Jackson, J. Mroz, G. Yoon and J. Baquero at the Bernard and Irene Schwarz Center for Biomedical Imaging, New York University, New York, NY, USA. We thank Dr. J. Bose of the University of Kansas Medical Center for providing *S. aureus* bacteria.

Funding

This work was funded in part by grants from the National Institutes of Health (HL139598, HL114477, HL131495, HL071544, HL130018, CA220234, HL144072, HL131478, EB017183 and NWO/ZonMW Vici 91818622); the American Heart Association (16SDG30190009, 16POST27030023); the Deutsche Forschungsgemeinschaft (KR4613/1-1) and the MGH Research Scholar Program.

References and Notes

1. Tong SY, Davis JS, Eichenberger E, Holland TL, Fowler VG, Staphylococcus aureus infections: epidemiology, pathophysiology, clinical manifestations, and management. Clin Microbiol Rev. 28(3),603–61 (2015). [PubMed: 26016486]
2. Cahill TJ, Baddour LM, Habib G, Hoen B, Salaun E, Pettersson GB, Schäfers HJ, Prendergast BD, Challenges in Infective Endocarditis. J Am Coll Cardiol. 69(3),325–344 (2017). [PubMed: 28104075]
3. Loeb L, The influence of certain bacteria on the coagulation of the blood. J Med Res. 10(3):,407–19 (1903). [PubMed: 19971581]
4. Friedrich R, Panizzi P, Fuentes-Prior P, Richter K, Verhamme I, Anderson PJ, Kawabata S, Huber R, Bode W, Bock PE, Staphylocoagulase is a prototype for the mechanism of cofactor-induced zymogen activation. Nature. 425(6957),535–9 (2003). [PubMed: 14523451]
5. Kroh HK, Panizzi P, Bock PE, Von Willebrand factor-binding protein is a hysteretic conformational activator of prothrombin. Proc Natl Acad Sci U S A. 106(19),7786–91 (2009). [PubMed: 19416890]
6. Panizzi P, Friedrich R, Fuentes-Prior P, Richter K, Bock PE, Bode W, Fibrinogen substrate recognition by staphylocoagulase.(pro)thrombin complexes. J Biol Chem. 281(2),1179–87 (2006). [PubMed: 16230339]
7. Panizzi P, Nahrendorf M, Figueiredo JL, Panizzi J, Marinelli B, Iwamoto Y, Keliher E, Maddur AA, Waterman P, Kroh HK, Leuschner F, Aikawa E, Swirski FK, Pittet MJ, Hackeng TM, Fuentes-Prior P, Schneewind O, Bock PE, Weissleder R, In vivo detection of Staphylococcus aureus endocarditis by targeting pathogen-specific prothrombin activation. Nat Med. 17(9),1142–6 (2011). [PubMed: 21857652]
8. Peetermans M, Liesenborghs L, Peerlinck K, Wijngaerden EV, Gheysens O, Goffin KE, Hoylaerts MF, Jacquemin M, Verhaegen J, Peeterman WE, Verhamme P, Vanassche T, Targeting Coagulase Activity in Staphylococcus aureus Bacteraemia: A Randomized Controlled Single-Centre Trial of Staphylothrombin Inhibition. Thromb Haemost. 118(5),818–829 (2018). [PubMed: 29614521]
9. Foster TJ, Immune evasion by staphylococci. Nat Rev Microbiol. 3(12),948–58 (2005). [PubMed: 16322743]
10. Panizzi P, Stone JR, Nahrendorf M, Endocarditis and molecular imaging. J Nucl Cardiol. 21(3),486–95 (2014). [PubMed: 24797384]
11. Sinusas AJ, Bengel F, Nahrendorf M, Epstein FH, Wu JC, Villanueva FS, Fayad ZA, Gropler RJ, Multimodality cardiovascular molecular imaging, part I. Circ Cardiovasc Imaging. 1(3),244–56 (2008). [PubMed: 19808549]
12. Weissleder R, Nahrendorf M, Advancing biomedical imaging. Proc Natl Acad Sci U S A. 112(47),14424–8 (2015). [PubMed: 26598657]
13. Schwaiger M, Kunze K, Rischpler C, Nekolla SG, PET/MR: Yet another Tesla? J Nucl Cardiol. 24(3),1019–1031 (2017). [PubMed: 27659455]
14. Ning X, Lee S, Wang Z, Kim D, Stubblefield B, Gilbert E, Murthy N, Maltodextrin-based imaging probes detect bacteria in vivo with high sensitivity and specificity. Nat Mater. 10(8),602–7 (2011). [PubMed: 21765397]
15. Hernandez FJ, Huang L, Olson ME, Powers KM, Hernandez KM, Meyerholz DK, Thedens DR, Behlke MA, Horswill AR, McNamara JO, Noninvasive imaging of Staphylococcus aureus infections with a nuclease-activated probe. Nat Med. 20(3),301–6 (2014). [PubMed: 24487433]
16. Pinkston KL, Singh KV, Gao P, Wilganowski N, Robinson H, Ghosh S, Azhdarinia A, Sevick-Muraca EM, Murray BE, Harvey BR, Targeting pili in enterococcal pathogenesis. Infect Immun. 82(4),1540–7 (2014). [PubMed: 24452680]
17. Yang CT, Ghosh KK, Padmanabhan P, Langer O, Liu J, Eng D, Halldin C, Gulyás B, PET-MR and SPECT-MR multimodality probes: Development and challenges. Theranostics. 8(22),6210–6232 (2018). [PubMed: 30613293]
18. Periasamy S, Joo HS, Duong AC, Bach TH, Tan VY, Chatterjee SS, Cheung GY, Otto M, How Staphylococcus aureus biofilms develop their characteristic structure. Proc Natl Acad Sci U S A. 109(4),1281–6 (2012). [PubMed: 22232686]

19. Vanassche T, Verhaegen J, Peetermans WE, Hoylaerts MF, Verhamme P, Dabigatran inhibits Staphylococcus aureus coagulase activity. J Clin Microbiol. 48(11),4248–50 (2010). [PubMed: 20810780]
20. Vanassche T, Verhaegen J, Peetermans WE, VAN Ryn J, Cheng A, Schneewind A, Hoylaerts MF, Verhamme P, Inhibition of staphylothrombin by dabigatran reduces Staphylococcus aureus virulence. J Thromb Haemost. 9(12),2436–46 (2011). [PubMed: 22040101]
21. Fournier PE, Casalta JP, Habib G, Messana T, Raoult D, Modification of the diagnostic criteria proposed by the Duke Endocarditis Service to permit improved diagnosis of Q fever endocarditis. Am J Med. 100(6),629–33 (1996). [PubMed: 8678083]
22. Mancini S, Oechslin F, Menzi C, Que YA, Claes J, Heying R, Veloso TR, Vanassche T, Missiakas D, Schneewind O, Moreillon P, Entenza JM, Marginal role of von Willebrand factor-binding protein and coagulase in the initiation of endocarditis in rats with catheter-induced aortic vegetations. Virulence. 9(1),1615–1624 (2018). [PubMed: 30280967]
23. Fowler VG, Proctor RA, Where does a Staphylococcus aureus vaccine stand? Clin Microbiol Infect. 20(5),66–75 (2014). [PubMed: 24476315]
24. Bose JL, Fey PD, Bayles KW, Genetic tools to enhance the study of gene function and regulation in Staphylococcus aureus. Appl Environ Microbiol. 79(7),2218–24 (2013). [PubMed: 23354696]
25. Scott PJH, Shao X, Fully automated, high yielding production of N-succinimidyl 4-[18F]fluorobenzoate ([18F]SFB), and its use in microwave-enhanced radiochemical coupling reactions. Journal of Labelled Compounds and Radiopharmaceuticals. 53(9),586–591 (2010).
26. Nahrendorf M, Keliher E, Marinelli B, Waterman P, Feruglio PF, Fexon L, Pivovarov M, Swirski FK, Pittet MJ, Vinegoni C, Weissleder R, Hybrid PET-optical imaging using targeted probes. Proc Natl Acad Sci U S A. 107(17),7910–5 (2010). [PubMed: 20385821]
27. Davis RW, Brannen AD, Hossain MJ, Monsma S, Bock PE, Nahrendorf M, Mead D, Lodes M, Liles MR, Panizzi P, Complete genome of Staphylococcus aureus Tager 104 provides evidence of its relation to modern systemic hospital-acquired strains. BMC Genomics. 17,179 (2016). [PubMed: 26940863]
28. Green N, Alexander H, Olson A, Alexander S, Shinnick TM, Sutcliffe JG, Lerner RA, Immunogenic structure of the influenza virus hemagglutinin. Cell. 28(3),477–87 (1982). [PubMed: 6176330]
29. Kohler G, Milstein C, Derivation of specific antibody-producing tissue culture and tumor lines by cell fusion. Eur J Immunol. 6(7),511–9 (1976). [PubMed: 825377]
30. Oi VT, Herzenberg LA, Immunoglobulin-producing hybrid cell lines, in Selected Methods in Cellular Immunology, Mishell BB, Shigi SM, Editor. Freeman: San Francisco 351–371 (1980).
31. Panizzi P, Friedrich R, Fuentes-Prior P, Kroh HK, Briggs J, Tans G, Bode W, Bock PE, Novel fluorescent prothrombin analogs as probes of staphylocoagulase-prothrombin interactions. J Biol Chem. 281(2),1169–78 (2006). [PubMed: 16230340]

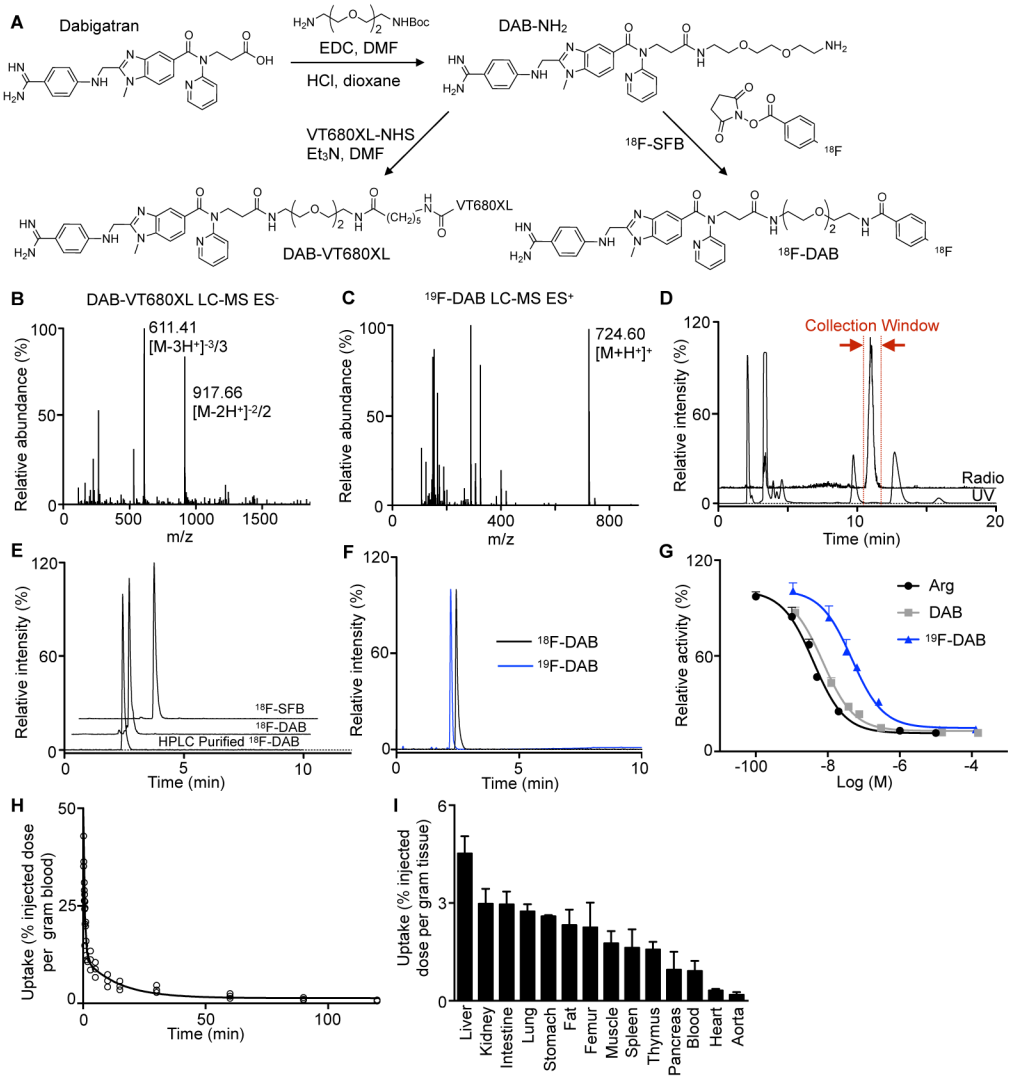

Fig. 1. Imaging agent synthesis and validation.

(**A**) Synthesis scheme of a near infrared fluorescent dabigatran derivative (DAB-VT680XL) and a positron emission tomography fluorine-18 tracer ^{18}F-dabigatran (^{18}F-DAB), both prepared in 2 steps from dabigatran. (**B**) LC-MS analysis of DAB-VT680XL showing the $[M - 2H^+]^{2-}/2$ (917.66 m/z) and $[M - 3H^+]^{3-}/3$ (611.41 m/z) ions and (**C**) ^{19}F-DAB showing the $[M + H^+]^+$ (724.60 m/z). (**D**) Preparative HPLC chromatograms (radio, top trace) and ultraviolet (UV) absorbance at 254 nm (bottom trace). The collection window is highlighted in red. (**E**) Analytical HPLC chromatograms of the ^{18}F-succinimidyl fluorobenzoate (^{18}F-SFB) prosthetic group, ^{18}F-DAB crude conjugation reaction mixture and HPLC purified ^{18}F-DAB. (**F**) Analytical HPLC chromatograms of ^{18}F-DAB and stable-isotope standard ^{19}F-DAB (blue). Since the two detectors are connected in series, there is a 0.2 min delay between UV and radio signals. (**G**) Thrombin activity assay with argatroban (Arg), dabigatran (DAB) and ^{19}F-dabigatran (^{19}F-DAB). (**H**) Clearing ^{18}F-DAB from mouse blood (n=3). The half-life in blood is 2.0±0.6 minutes. (**I**) Bio-distribution of ^{18}F-DAB in mice (n=3-8). Data are shown as mean ± s.e.m..

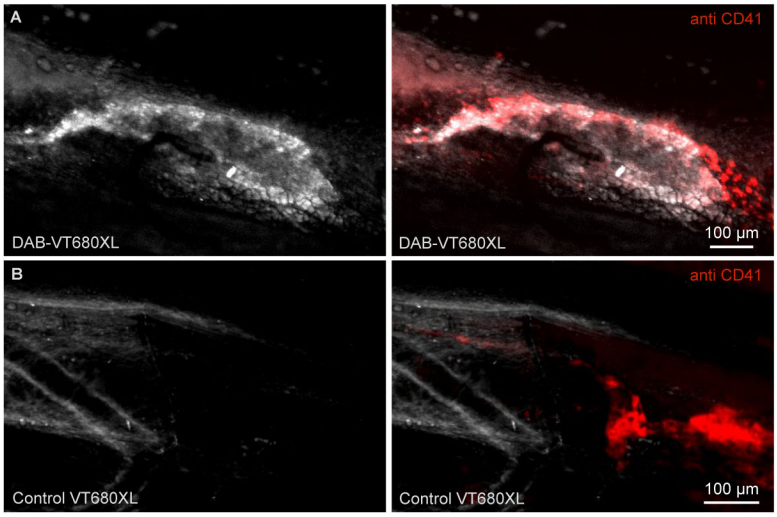

Fig. 2. In vivo DAB-VT680XL or control probe binding to thrombi in mice.

(**A**) Intravital microscopy of a $FeCl_3$-induced thrombosis of the femoral artery 90 min after injection of DAB-VT680XL or (**B**) an unspecific control fluorochrome (VT680XL). Aggregating platelets are stained with anti-CD41 monoclonal antibody (red). The experiments were repeated twice with the same result (n=3 per group).

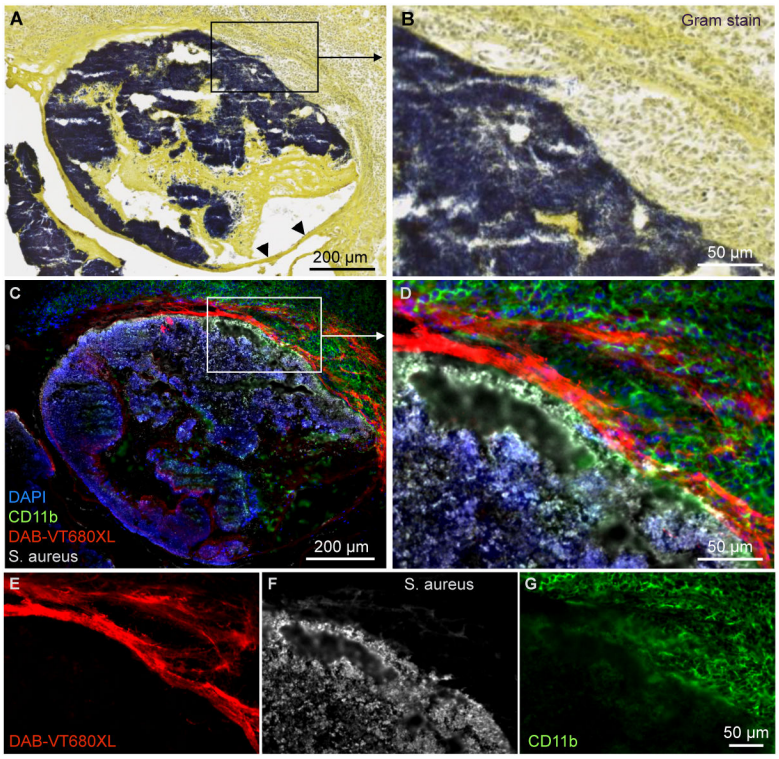

Fig. 3. DAB-VT680XL targeting of endocarditic vegetations in mice.

(**A**) Gram stain of aortic root after inducing endocarditis in mice shows *S. aureus* in dark purple. Arrow heads indicate aortic valve leaflet. (**B**) High magnification view of boxed area in (A). (**C, D**) Adjacent sections of the endocarditic vegetation 90 min after DAB-VT680XL injection. DAPI indicates 4′,6-diamidino-2-phenylindole. DAB-VT680XL imaging signal (**E**) highlights the intersection of bacterial vegetations (**F**) with the host. Staining for CD11b (**G**) illustrates the distribution of myeloid cells, which are unable to enter the bacterial colony. The experiment was repeated twice with the same result.

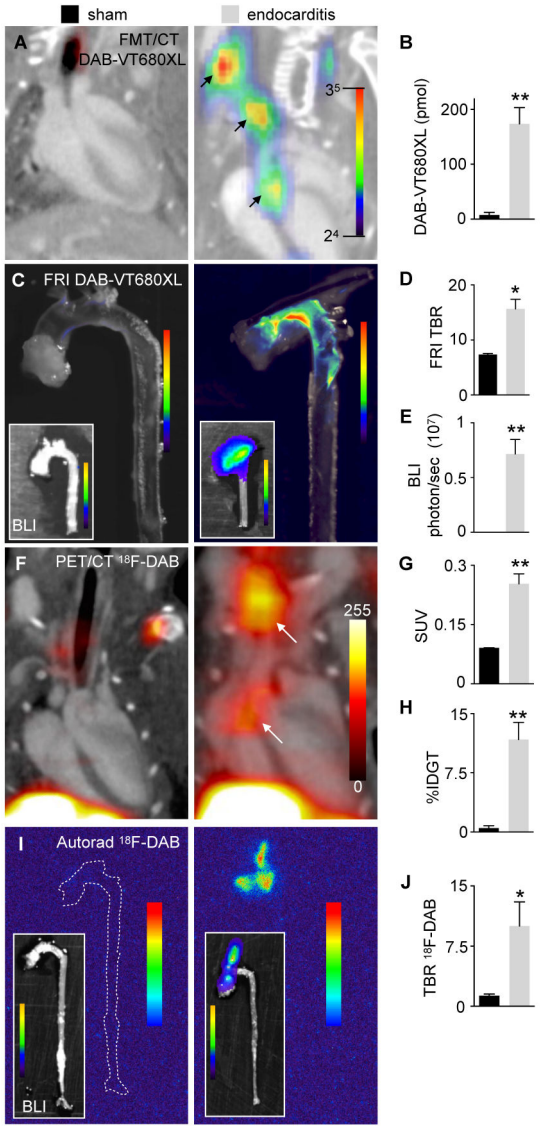

Fig. 4. Noninvasively imaging mouse endocarditis.

(**A**) In vivo FMT/CT images and (**B**) fluorescence quantification in the aortic roots of mice with *S. aureus* endocarditis (right) and sham controls (left) (n=5-8 mice per group; $P = 0.0055$). (**C**) Ex vivo fluorescence reflectance imaging (FRI) and bioluminescence imaging (BLI, insets) illustrate macroscopic co-localization of bacterial colonies with DAB-VT680XL imaging signal. (**D**) Quantification of fluorescence as target to background ratio (TBR) (n=5-8 mice per group, $P = 0.0286$). (**E**) Quantification of BLI signal derived from bioluminescent *S. aureus* strain Xen29 (n=5-8 mice per group, $P = 0.0095$). **(F)** PET/CT imaging after injection of ^{18}F-DAB. Arrows indicate signal from *S. aureus* vegetations on the aortic valves and the suture in the brachiocephalic artery. (**G**) In vivo quantification of PET signal in the aortic root (SUV, standardized uptake value, n=6-10 mice per group, data from four separate experiments, $P = 0.0095$). (**H**) Ex vivo scintillation counting of aortic roots (%IDGT, percent injected dose per gram tissue, n=5-12 mice per group, $P = 0.0052$). (**I**) Autoradiography of dissected aortas. Left panel, sham-operated mouse with absent ^{18}F-

DAB signal and absent bioluminescent signal indicating lack of bacteria; right panel with ^{18}F-DAB signal with co-localized bioluminescent bacterial colonies in the ascending aorta (inset). (**J**) Quantification of autoradiography (TBR, target to background ratio, n=5-7 mice per group, three separate experiments, $P = 0.037$). Unpaired, two-tailed t-test was used and data are shown as mean ± s.e.m.. $^{*}P < 0.05$, $^{**}P < 0.01$.

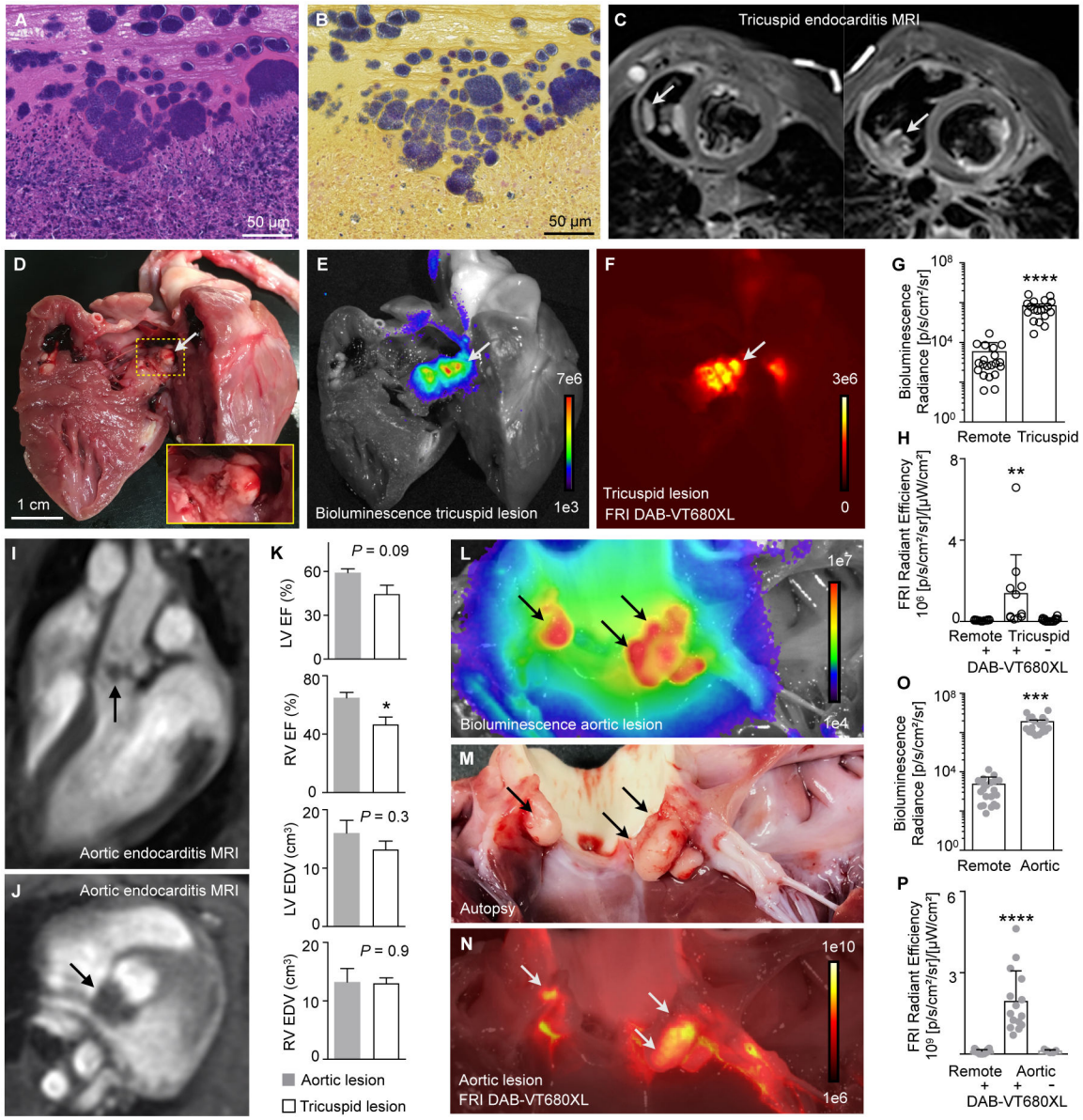

Fig. 5. *S. aureus* endocarditis in piglets.

(**A**) H&E staining of right-sided piglet endocarditis vegetation indicating immune response to the *S. aureus* Xen 36 infection. (**B**) Gram staining of an adjacent section showing the pathogen in the piglet heart. (**C**) Short axis stacks of black blood MRI from a pig 10 days after induction of right-sided endocarditis. Arrows indicate vegetations. (**D**) View of the open right ventricle in piglet with right-sided endocarditis. Inset shows magnified view. (**E**) Bioluminescence image of (D) illustrates location of Xen 36 *S. aureus*. (**F**) Fluorescence reflectance image (FRI) of (D) and (E) indicates DAB-VT680XL imaging signal after intravenous injection of the near infrared imaging agent. (**G**) Ex vivo quantification of bacterial bioluminescence from multiple vegetations of 12 piglets with right-sided endocarditis. Unpaired, two-tailed t-test was used and data are shown as mean ± s.e.m., ****$P < 0.0001$. (**H**) FRI in a DAB-VT680XL-injected subset of piglet demonstrates

accumulation of the imaging probe (n=3 piglets per group, one-way ANOVA for multiple comparison, Barlett's test, $^{**}P < 0.01$. (**I**) Long and (**J**) short axis MRI of piglet after induction of left-sided endocarditis. (**K**) Cardiac MRI-derived ejection fraction (EF) of the right and left ventricle (RV and LV, respectively) and the end-diastolic volumes (EDV), comparing left- with right-sided endocarditis (n=6 piglets with tricuspid right-sided and n=4 with aortic left-sided disease, two tailed t test, $^{*}P < 0.05$). (**L**) Bioluminescence imaging demonstrates bacterial infection, with signal arising from vegetations (arrows) identified on autopsy (**M**) and FRI (**N**). (**O**) Ex vivo quantification of bacterial bioluminescence in 8 piglets with left-sided endocarditis, two-tailed t test., $^{***}P < 0.001$. (**P**) Quantification of fluorescence signal arising from aortic valve vegetations (n=5 piglets, one-way ANOVA for multiple comparison with $^{****}P < 0.0001$, Barlett's test).

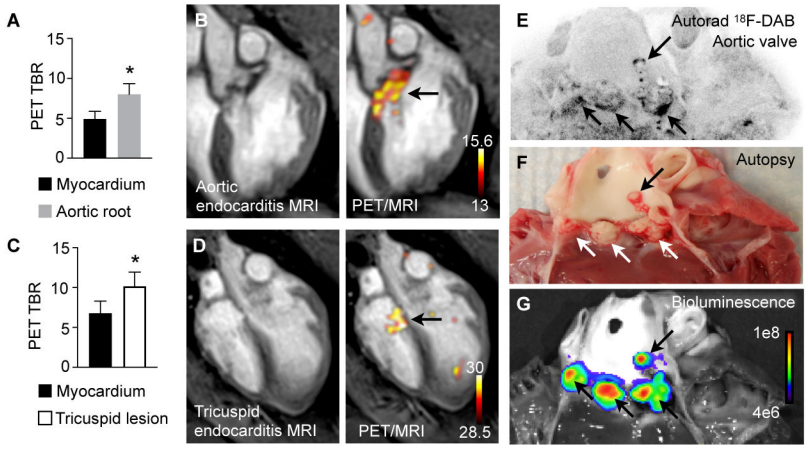

Fig. 6. PET/MR imaging *S. aureus* endocarditis in piglets.

(**A**) Left-sided endocarditis target to background ratio (TBR) of PET signal, calculated with either myocardium (control) or vegetation-bearing aortic root as target and the skeletal muscle as background (n=3 piglets, two-sided Student's t test, $*P < 0.05$). (**B**) PET/MR images illustrating the imaging signal in aortic valve with endocarditis lesion (arrow). Color scale depicts becquerels/mL. (**C**) Right-sided endocarditis TBR, calculated as above (n=3 piglets, two-sided Student's t test, $*P < 0.05$). (**D**) PET/MR images illustrating the imaging signal in tricuspid valve endocarditis lesion (arrow). Color scale depicts becquerels/mL. (**E**) Ex vivo autoradiography of aortic valve indicates radioactive signal in the aortic valve vegetations, which were verified on autopsy (**F**) and a source of bioluminescence (**G**) arising from *S. aureus* (arrows).

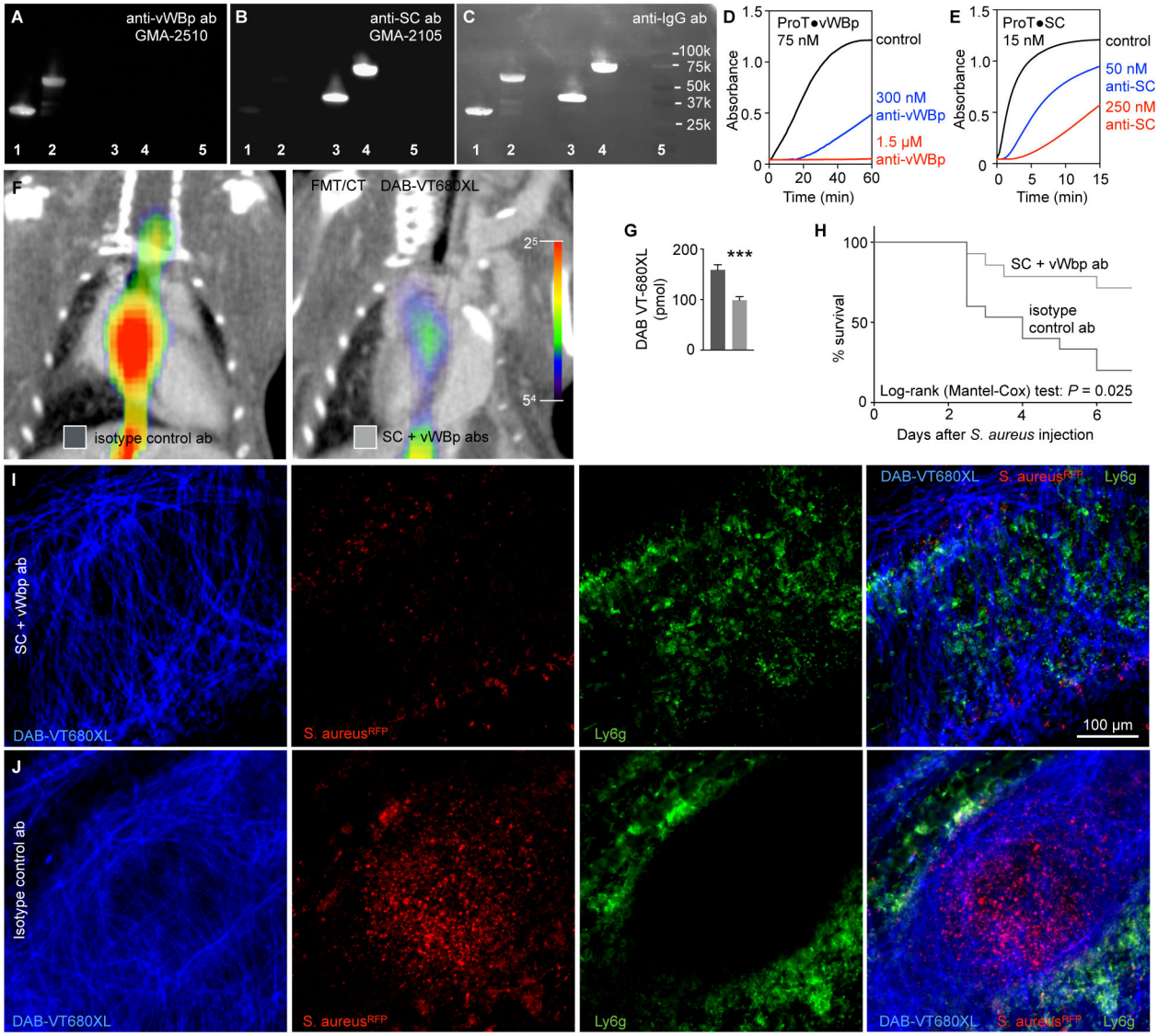

Fig. 7. Immunotherapy neutralizing virulence factors disrupts vegetations and improves survival.

(**A-C**) Specificity of monoclonal antibodies by immunoblotting against vWBp-(1-263) in lane 1; vWBp-(1-474) in lane 2; SC-(1-325) in lane 3; SC-(1-660) in lane 4. Lane 5 contains protein standards with the indicated molecular weights. The indicated antibodies, in panel A GMA-2510 monoclonal [*anti*-von Willebrand factor-binding protein (*anti-vWBp*)] and in panel B GMA-2105 monoclonal [*anti*-staphylocoagulase (*anti-SC*)], are specific for their respective targets. Panel C shows probing for total mouse IgG (*anti-IgG* polyclonal against both the heavy and light chains of murine IgG) and reflects the bound antibodies shown in panels A and B. (**D**) Increase in turbidity as measured by absorbance change at 450 nm for mixtures of 1.5 mg/mL fibrinogen and 75 nM prothrombin complexed to vWBp-(1-263) (*ProT●vWBp*) complex in the absence of GMA-2510 antibody (*anti-vWBp Ab*; black line), in the presence of 300 nM anti-vWBp Ab (blue line) or 1.5 µM anti-vWBp Ab (red line). (**E**) Similar reactions for 15 nM prothrombin complexed to SC-(1-325) (*ProT●SC*) are shown in

the absence of GMA-2105 antibody (*anti-SC Ab*; black line), in the presence of 50 nM anti-SC ab (blue line) or 250 nM anti-SC ab (red line). (**F**) In vivo FMT/CT images of *S. aureus* endocarditis in mice after injection of DAB-VT680XL treated with either isotype control antibody or antibodies neutralizing SC and vWBp. (**G**) In vivo fluorescence quantitation of vegetation thrombin in aortic roots following DAB-VT680XL injection (n=10-12 mice per group, three separate experiments; unpaired, two-sided t-test was used and data are shown as mean ± s.e.m. ***$P < 0.001$). (**H**) Kaplan-Meier survival curves of *S. aureus* endocarditis mice treated with isotype control antibody or combination therapy with anti-SC and anti-vWBp antibodies (n=15 mice per group, mice received a single intraperitoneal injection of their respective antibody treatment 6 hrs post surgery). (**I**) Intravital microscopy of femoral *S. aureus* vegetation 24 hours after intravenous injection of *S. aureus*$^{RFP+}$ and combination treatment with both anti-SC and anti-vWBp or (**J**) isotype control antibody. In vivo DAB-VT680 microscopy of the vegetation wall surrounding RFP^+ bacteria and $Ly6g^+$ neutrophils.